# Tailoring Surface and Bulk Morphologies to Control Transport Properties of Sulfonated Block Copolymer Films

Karthika Madathil,[y] Banafsheh Hekmatnia,[z] Haleh Ardebili,[{,z] and Gila E. Stein*[,y]

yDepartment of Chemical and Biomolecular Engineering, The University of Tennessee at Knoxville, Knoxville, Tennessee 37996, United States

zMaterials Science and Engineering Program, The University of Houston, Houston, Texas 77204, United States

{Department of Mechanical Engineering, The University of Houston, Houston, Texas 77204, United States

E-mail: gstein4@utk.edu

## Abstract

We examine the eects of solvent composition and solution-casting protocol on the structure of a lamellar sulfonated pentablock copolymer (SPC) membrane. Films are prepared by a layering process, wherein the lm is built up through sequential bar-coating steps. Process variables include bar gap height, which controls drying time and layer thickness, and solvent selectivity toward each block in the SPC, which controls solution-state structure and biases the domain orientations at the surface. We nd that irrespective of solvent selectivity, one-layer lms have poorly ordered structures in the bulk with minimal restructuring near the surface. However, when the process involves sequential deposition of two or more layers, then the bulk structure of dry lms can be well-predicted by the solution-state structure, and domain orientations at the

surface are templated by polymer-solvent interactions. Consequently, processing conditions strongly inuence through-plane transport properties of the SPC lms. When the casting process generates disordered lamellae in bulk with a perpendicular lamellar orientation at the surface, both water and protons can move across the lm. However, when the process generates highly ordered lamellae in bulk and parallel lamellar orientations at the surface, transport of both water and protons is inhibited by limited pathways. Signicantly, the methodology outlined in this work can be extended to other ionic block copolymer platforms, allowing researchers to tailor bulk and surface morphologies for optimization of critical transport properties.

Key words: Block copolymer, orientation, membrane transport, conductivity, anisotropy

## Introduction

Ionic block copolymers show promise for applications such as membranes for fuel cells and batteries,[15] water purication,[610] and gas separation.[9,11] In these polymers, one of the blocks contains ionic or strongly acidic species that provides pathways for water and ion transport, and the other non-polar block (or blocks) tailor the mechanical properties. For instance, in sulfonated block copolymers, transport of water, methanol and protons is controlled by the composition and continuity of the sulfonated block.[9,12,13] Broadly, it has been shown that the transport properties of ionic block copolymers depend on the connectivity of the ionic domains.[1417] For example, the gyroid morphology with 3D interconnected networks has been shown to be highly ecient for ion conduction.[18,19] Lamellar morphologies with poorly ordered, randomly oriented grains are shown to have better domain connectivity and thus higher ionic conductivity as compared to well-ordered lamallae with large grain sizes.[16,17] In the poorly ordered lamellar morphology, a high density of branching defects along with small grain sizes result in network-like structures with well-connected domains and low tortuosity.[16,17,20,21] On the other hand, cylindrical morphologies with 1D ion transport pathways[22,23] and disordered ionic domains with limited connectivity[24] have poor

transport properties. Thin lms of ionic block copolymers are often prepared with solvent-based processing, as it can be dicult to activate self-assembly with thermal annealing due to slow inter-block chain diusion due to strong incompatibility between blocks and multiblock architectures. Solvent processed lms have non-equilibrium structures determined by several parameters such as the polarity of the solvent and the solvent evaporation rate.[12,25,26] Understanding process-structure relationships is thus necessary for designing ecient membranes based on ionic block copolymers.

Sulfonated block copolymers, consisting of sulfonic acid groups tethered to one of the blocks, are a promising material platform for fuel cells.[27,28] In particular, a sulfonated pentablock copolymer (SPC) with the trade name Nexar has been extensively studied as a low cost, environmentally friendly alternative to the sulfonated uorocarbon-based copolymers that are the current benchmark material for proton-exchange membrane fuel cells.[27,28] Nexar, or poly(tert-butylstyrene-b-hydrogenated isoprene-b-sulfonated styrene-b-hydrogenated isoprene-b-tert-butylstyrene) (tBS-HI-SS-HI-tBS), consists of a partially sulfonated styrene mid-block that can take up water and act as channels for water and ion/proton transport. The partially sulfonated midblock is attached to glassy poly(tert-butyl styrene) end-blocks via a hydrogenated polyisoprene linker, which prevents uncontrolled swelling and imparts the membrane with mechanical integrity and toughness. Previous works have studied the self-assembly of Nexar in solutions of varying solvent polarity[12,2932] and the nal lm structure obtained after solvent casting and drying.[12,24,3335] These works have demonstrated that the nal lm structure can be partly controlled by the pre-assembled structure in the solution. The translation of structure from solution to lm is also dependent on the casting process. As an example, previous work from our group showed that for lms prepared by bar-coating, the nal lm structure depends on the gap height of the bar.[36] Solutions having a well-dened lamellar structure produced lms with poorly ordered domains when cast using a low gap height, but produced lms with ordered lamellae when the gap height was increased to 1000 µm. By increasing the gap height, we are essentially

increasing the drying time and allowing the polymer chains more time to transition from the solution structure to lm structure. Films with lamellar structures could also be achieved by using the process of sequentially depositing layers of polymer solution after the previously deposited layers are dried. When a new layer is deposited, solvent can diuse into the underlying dry lm, re-exposing the polymer chains to the solvent and thus providing mobility for rearrangements. Consequently, both the gap height and the number of deposited layers impacts the nal lm structure.[36]

Self-assembled ionic block copolymers can also develop domains with a preferred orientation during solvent processing.[13,37] Such orientation eects are known to result in anisotropy in ion transport properties in the through-plane and in-plane direction.[3844] Specically, for self-assembled structures with 2D conducting pathways such as lamellae, the orientation of domains parallel to the plane of the lm depresses the conductivity in the through-plane direction compared to the in-plane direction.[42,43,45,46] A previous study on solution-cast SPC lms showed that lms cast from a moderately polar solvent (tetrahydrofuran) had well-ordered lamellar structures with directional anisotropy, whereas lms cast from a non-polar solvent (cyclohexane/heptane mixture) had a disordered morphology of isolated SS domains with less anisotropy,[47] but the physics that drive these dierent behaviors were not discussed.

In this work, we examine the process parameters that control both the kinetics and thermodynamics of SPC self assembly during lm processing. Both the bulk and surface structures of the lms are examined as a function of deposition conditions and solvent quality, and then compared with through-lm measurements of proton conductivity and water vapor transport rates. We show that under certain conditions, the lm morphology can be predicted from the solution-state structure, akin to a templating eect. We also propose that structural anisotropy in these materials is a consequence of preferential polymer-solvent interactions at the skin layer, and consequently, the domain orientations can be tailored through judicious selection of solvent composition. The methodology outlined in this study oers a path to produce the ideal surface and bulk structures for through-lm transport.

# Experimental

SPC Material The sulfonated pentablock copolymer (SPC), poly(tert-butylstyrene-b-hydrogenated isoprene-b-sulfonated styrene-b-hydrogenated isoprene-b-tert-butylstyrene) (tBS-HI-SS-HI-tBS) was provided by Kraton Polymers as lms.[48] The midblock styrene was sulfonated to 52 mol% per the manufacturer. The weight fractions of the SPC blocks were 20-10-40-10-20 (tBS-HI-SS-HI-tBS) and the overall molecular weight was approximately 60 to 70 kg/mol. The as-received lms had a spherical morphology with an SS core and tBS/HI matrix, as reported by others[37,49] and conrmed with SAXS measurements. The lms were soaked in deionized water (18.2 MW) for 24 hours to extract byproducts from the sulfonation reaction, then dried in air for 24 hours.

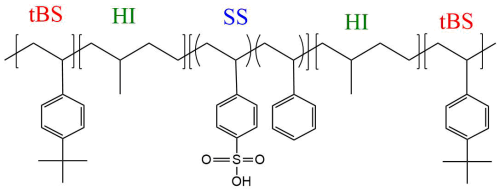


Figure 1: Structure of SPC, where tBS = tert-butylstyrene, HI = hydrogenated isoprene, and SS = partially sulfonated styrene (52 mol%). Molecular weight (pre-sulfonation): 15-10-28-10-15 kg/mol.

Polymer Solution and Film Preparation Polymer solutions were prepared by dissolving the polymer in a mixed solvent of Toluene (T, ACS grade, Fisher) and n-Propanol (nP, 99.0%, VWR). The solvents are denoted as nP_X, where X is the wt% of n-propanol in the nP/T solvent mixture. The amount of water taken up by the lm under ambient humidity was determined prior to polymer dissolution by measuring the mass of the sample after drying and again under ambient humidity. Water was then added to the polymer solutions to adjust the value of to 8, where = moles of water: moles of sulfonic acid group. This step was done to ensure that all the solutions have the same value of , as we saw in our previous work that self-assembly kinetics and domain periodicity in the solution are strongly inuenced by the amount water present in the solution.[36] The solutions were allowed to

stand for two days before performing SAXS measurements. All lms were cast on a Mylar sheet, in a controlled humidity chamber maintained at (55 2)% RH, using an Elcometer lm applicator with dierent gap heights ranging from 100 µm to 1000 µm. Two- and three-layer lms were prepared by sequential coating steps, wherein a new layer of solution was deposited after the previous layer was allowed to dry in the controlled humidity chamber.

Small-Angle X-ray Scattering (SAXS) A Xenocs GeniX 3D microfocus source with a copper target was used to produce a monochromatic beam with a 0.154 nm wavelength. The sample to detector distance was 0.9 m. A Pilatus3 R 300K detector (Dectris) with nominal pixel dimensions of 172 m 172 m was used for data acquisition. The data acquisition time was 3 min for all measurements. In all the gures showing SAXS data, the plots from each data set have been vertically oset for clarity. Samples were mounted vertically for transmission-mode measurements and horizontally for grazing-incidence (GI) mode. In the latter, the angle of incidence was set to 0.05 °to probe the near-surface structure; however, considering the high roughness of the lms, there is actually a distribution of incident angles that is not that well-dened.

Transmission Electron Microscopy (TEM) TEM measurements were performed on lms that were sectioned to a thickness of around 30 nm by a Leica EM FC7 microtome at -30 C. The sections used for TEM imaging were extracted at a depth of 5-50 µm, obtained by rst removing several micrometer-thick sections from the surface of the lm. The sections were stained by placing them in a solution of aqueous lead acetate for 7 hours, which selectively stains the sulfonated styrene domain. The obtained sample slices were imaged by a JEOL JEM 1400-Flash transmission electron microscope with an acceleration voltage of 120 kV.

Water Vapor Transport Rate Water vapor transport rate was measured using the upright vial method at 22°C and RH below 10%. 1 ml of DI water was added to 4 ml vials,

leaving head space over the water. The lm samples were tightly fastened between the vial and the cap in order to create a semipermeable seal for water vapor transport. Additionally, a paralm seal was tightly wrapped around the lower edge of the cap to minimize water escape through any pathway other than through the lm. The fastening of the cap and para lm was done within 10-15 sec of placing the lm on the vial, and the vial was immediately placed on a weighing scale. Mass was recorded over a period of 1 hour and then mass loss was calculated relative to the initial measurement (at 10-15 sec).

Water Uptake Water uptake was calculated using Eq. 1. $W_{dry}$ refers to the mass of the lm after drying in the oven for 12 hrs at 90°C. The lms were weighed within 10 sec after removal from the oven. $W_{humid}$ for samples under ambient conditions refers to the mass of the samples after equilibrating at ambient temperature (25°C) and humidity (34% RH) for more than an hour. $W_{humid}$ for samples soaked in water refers to the mass of samples after equilibrating at ambient conditions, followed by soaking in DI water for 10 minutes.

$$\text{Water uptake (\%)} = \frac{W_{humid} \quad W_{dry}}{W_{dry}} \; 100 \tag{1}$$

Electrochemical Impedance Spectroscopy For measurements of samples with low water uptake (25 and 50 wt%), the lms were allowed to equilibrate at ambient temperature (25°C) and humidity (34% RH) for over an hour. Samples used for measurements were obtained by cutting out circular disks (A = 0.94 $cm^2$) from the lms. Film thickness was measured using a caliper with an accuracy of 10 µm. The lms were sandwiched between two stainless steel electrodes to obtain a through-lm conguration. Data were collected over a frequency range of 10 Hz to 1M Hz and 10 mV amplitude. Nyquist plots made using these data are shown in Figure s8. As there were not many points in the semicircle region of the Nyquist plot, which is needed to obtain a good t to an electrical circuit model, the bulk resistance was estimated by extrapolating a straight line from the beginning of the

semicircle to obtain the Z' intercept where -Z is zero, as shown in the insets of Figure S8. For measurements of samples with high water uptake (greater than 100 wt%), the samples equilibrated at ambient humidity were soaked in water for 10 min, and this produced a water uptake in excess of 100 wt% relative to dry lm mass. Thicknesses of these samples were measured after taking the soaked samples out of water and patting dry with a wipe.

## Results and Discussions

The objective of this work is to understand how lm processing protocols can tailor the surface and bulk structures of the lm, which in turn impacts water and proton transport within the lm. We explore a layering process, wherein the lm is deposited through sequential bar-coating steps with variable bar gap height, as well as two solvent compositions that have dierent selectivities towards the SPC blocks. The lms were cast using 1000 µm or 100 µm gap heights and prepared by depositing one (1000 µm), two (1000 µm2), or three-layers (1000 µm3 and 100 µm3). Note that we could not blade-coat lms with a gap height that is larger than ca. 1500 µm because the solution is not viscous enough to ll a large gap between the blade and substrate. The nP_30 solvent is selective to the tBS and HI blocks, while the nP_50 solvent is approximately neutral to all blocks.[12,50] The calculated Hansen solubility parameters for both solvent mixtures and the interaction distance ($R_a$) between each mixed solvent and the distinct polymer blocks is reported in Table S1. All the lm structures discussed in the following sections were cast from solutions containing 15 wt% SPC in the solution. SAXS data were collected in two dierent congurations, k and ?, as shown in Figure 2.

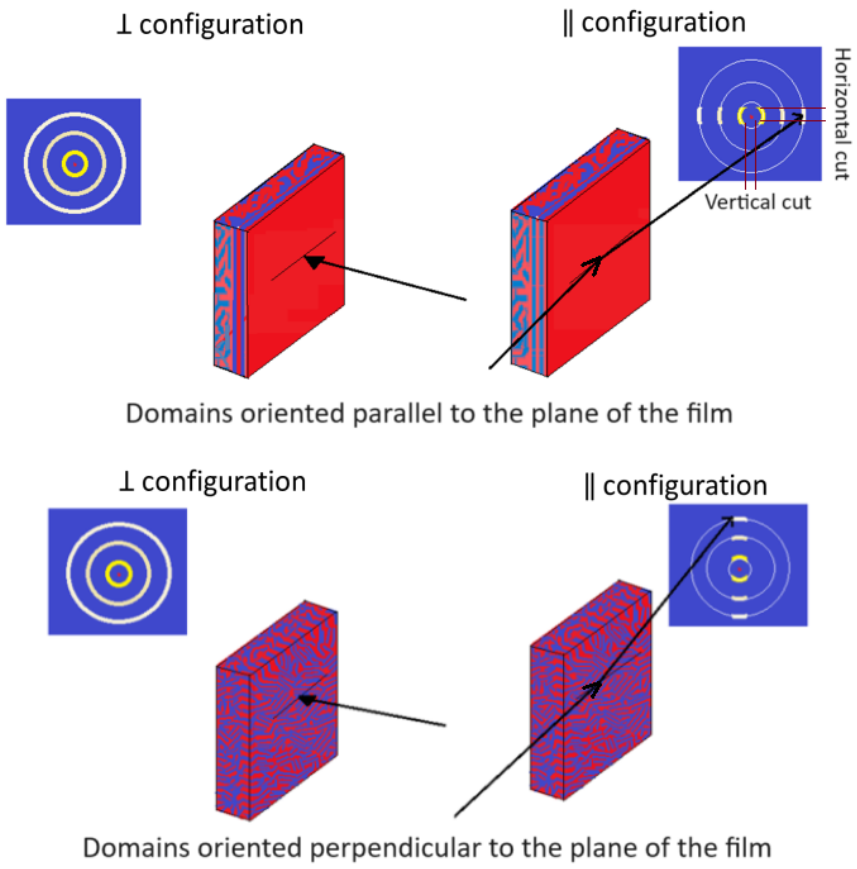


Figure 2: Illustration for the '?' and 'k' SAXS measurement congurations for domains oriented parallel and perpendicular to the plane of the lm, where the arrow represents the direction of the X-ray beam. The regions marked 'vertical cut' and 'horizontal cut' contain scattering from domains that are oriented perpendicular and parallel to the plane of the lm, respectively.

## Bulk Structure

Figure 3 reports the SAXS data that were collected using the '?' conguration. The nP_30 solvent composition resulted in a cylindrical solution structure with a periodicity of 49 nm, and is near the border of the cylinder-to-lamellar phase boundary wherein a transition to the LAM phase occurs with an increase in nP content of the solvent (Fig. S1 and S2). Figure 3a shows the SAXS data for the lms cast from the nP_30 solvent. For the lms cast using this solvent composition and a 1000 µm gap height, SAXS measurements of the one-layer lm show a poorly ordered structure with a primary peak at $q^{?}$ = 0:136 $nm^{-1}$, corresponding

to a periodicity of 46.2 nm, and a broad secondary peak. The SAXS prole and periodicity of this one-layer lm is the same as that of the one-layer lm cast with a 250 µm gap, shown in Figure S3. SAXS measurements of the two-layer lm show an ordered lamellar structure with three higher order peaks and a domain periodicity of 43.6 nm. The three-layer lms cast using both 1000 µm and 100 µm gap heights showed an ordered lamellar structure with a periodicity of 41.6 nm. TEM data for a three-layer lm cast with a 1000 µm gap height are shown in Figure 4a, conrming the ordered lamellar structure. These experiments show that sequential deposition steps improve lamellar order, irrespective of gap height.

Figure 3b shows the SAXS data for the lms cast from the nP_50 solvent. The nP_50 solutions produced a scattering prole characteristic of solutions composed of dissolved polymer chains, rather than a self-assembled structure (Figure S2). The SAXS data for all lms cast from this solvent show a scattering peak at $q^?$ in the range of 0.144 to 0.167 $nm^{-1}$, corresponding to length scales between 43.6 and 37.5 nm, along with oscillations in intensity at higher q that arise from the form factor. We plot the lamellar form factor in Figure 3b for the 100 µm3 lm using 39.3 nm as the periodicity, which is calculated from $q^?$ = 0:159 $nm^{-1}$, and a domain width of 29.5 nm. TEM data for a three-layer lm cast with a 1000 µm gap height are shown in Figure 4b, conrming the disordered lamellar structure. In contrast to lms cast from nP_30 solvent, sequential deposition steps have little impact on lamellar order on the lms cast from nP_50 solvent.

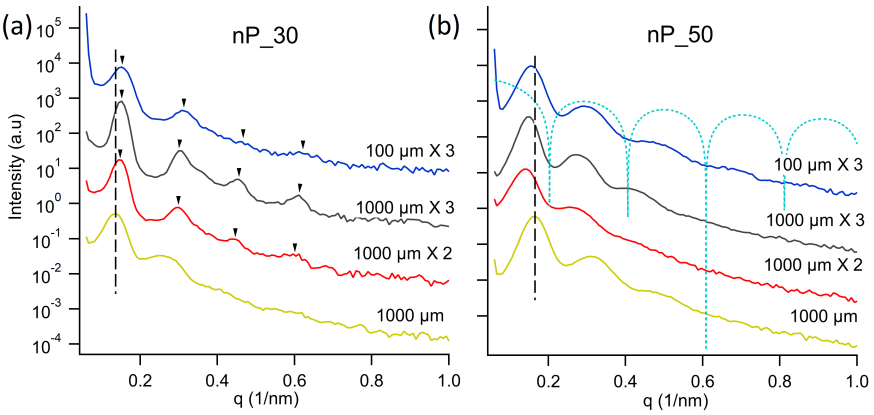


Figure 3: Transmission SAXS of lms cast using 1000 µm gap height by depositing one, two (2), and three (3) layers, and 100 µm gap height by depositing three (3) layers. (a) Films cast from nP_30 solvent, and (b) lms cast from nP_50 solvent. The inverted triangles indicate peak positions for the ordered lamellar morphology.

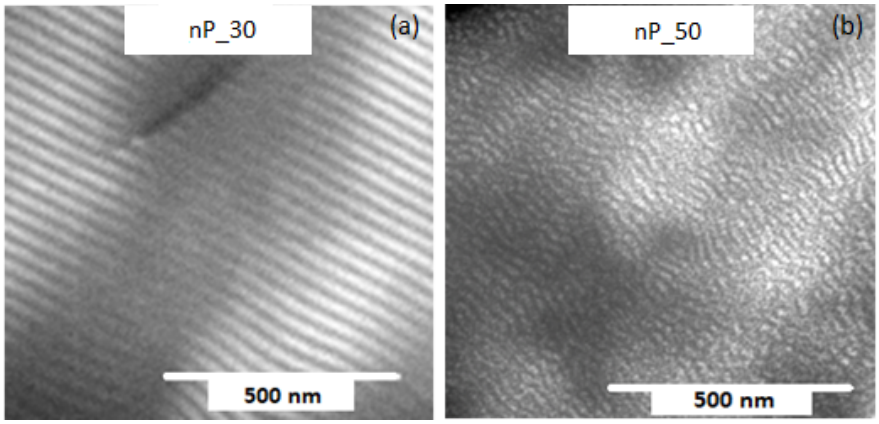


Figure 4: TEM images for three-layer lms cast using the 1000 µm gap height. The dark region corresponds to the SS domains and light regions correspond to the tBS/HI domains. a) Cast from nP_30 solvent; and b) Cast from nP_50 solvent.

These results show that lm structure is inuenced by the solvent composition, solution-state structure, and the casting process. The three-layer lms cast from the nP_30 solvent, with the solution composition near the boundary of lamellar and cylindrical phase, form a highly ordered lamellar morphology, whereas the lms cast from the nP_50 solvent, with no self-assembled structure in solution, form a poorly ordered network-like morphology. In the sequential deposition process, it appears that solution-state structure is a reasonable predictor of the lm morphology, akin to a templating eect. A similar templating eect

was observed in a prior work where solution-cast SPC lms were prepared by a sequential deposition process.[12] One-layer lms, on the other hand, show a poorly ordered structure when cast from either neutral or tBS/HI selective casting solvents. This loss of the templating eect for one-layer lms cast was investigated for a broad range of solution compositions, as shown in the Supplementary Information (Figures S1-S3), for a low gap height. In brief, we nd a poorly ordered structure for a broad range of casting solution compositions, despite the fact that the solution-state structures are dierent. TEM data for select lms are shown in Figure S4, which reveals a disordered structure comprised of SS domains in a matrix of tBS/HI. In a previous work, we showed that when lamellar SPC solutions are cast into lms with the one-layer process, a poorly ordered structure is produced with low gap heights but ordered lamellar domains are produced with large gap heights (1125 μm) or by drop-cast thick lms (ca. 300 μm).[36] We conclude that when lms are cast with a one-layer process, a minimum drying time is required to template the structure from solution to lm. During drying, the domain periodicity in the self-assembled structure changes as the solvent evaporates, and very fast drying seems to disrupt the morphology during this process. We note that very slow drying also results in a lm structure that diers from the solution structure, as the self-assembled morphology will adjust in response to the changing solution composition and polymer concentration. In Figure S5, we show SAXS measurements of lms produced by drop casting from a lamellar solution and dried by a fast (< 1 hr) versus slow (days) evaporation processes at ambient conditions. The fast drying leads to a lamellar structure, while slow drying produces a poorly ordered structure. Therefore, we also conclude that there is also an upper bound to the drying time for a one-layer templating process.

The domain periodicities in lms dier as a function of solvent composition, even when the lms have the same poorly ordered morphology. In the solution phase, the swelling of the blocks depends on the solvent composition, and the domains may expand or contract to move towards their equilibrium periodicity as the lm dries. The non-polar solvent composition, nP_30, is expected to cause greater swelling of both the SS and the tBS/HI domains,

compared to the neutral solvent composition of nP_50.[31] This is because an increase in the fraction of non-polar solvent results in greater segregation of the polar solvent into the hydrophilic domain and the non-polar solvent into the hydrophobic domain, resulting in greater stretching of both the polar and non-polar domains. This could be the reason why the periodicity of the poorly ordered structure in the lm cast using 1000 µm gap height from the nP_30 solvent (46.2 nm) is much larger than that of the lm cast from the nP_50 solvent (37.5 nm). During sequential deposition of layers, we are increasing the solvent exposure time of the previously deposited layers to provide mobility for rearrangement. From Figure 3, we observe that lms cast with sequential layering from the nP_30 and nP_50 solutions have smaller and larger periodicities, respectively, compared to lms cast with a one-layer process.

## Surface Structure

Next, we study how the sequential deposition of layers can result in the formation of oriented domains in the surface layer of the solution cast SPC. During lm drying, the surface layer is depleted of solvent due to rapid evaporation at the air/polymer interface.[51,52] This results in the formation of a 'skin layer' at the surface, and the solvent trapped in the bulk of the lm depletes via diusion through this polymer-rich skin layer. The formation of oriented domains during solvent removal is known to depend on the solvent evaporation rate.[53,54] While rapid solvent evaporation can trap unoriented domains from the solution in the dry lm, the solvent evaporation rate has to be suciently fast to cause a gradient of solvent concentration along the lm thickness, resulting in orientation of domains along the concentration gradient. We hypothesize that the polymer domains in the skin layer will show a preferential orientation depending on solvent selectivity, due to the sharp change in solvent concentration at the bulk/skin interface, whereas the domains in the bulk would remain unoriented. To check for a preferred orientation of domains with respect to the plane of the lm, SAXS measurements were performed in the 'k' conguration as shown in Figure

2a. Note that while the SAXS measurements in the 'k' conguration show the presence of oriented domains in the lm, this technique does not establish the location of the oriented domains within the lm. However, it is logical to assume that the oriented domains, if present, are on the surface of lm. This assumption is conrmed through grazing-incidence SAXS measurements (GISAXS) on select lms, which are reported in Figure S6.

Figure 5 shows the 2D SAXS pattern for measurements performed in the 'k' conguration for one-layer (1000 µm) and three-layer (1000 µm3 and 100 µm3) lms cast from both nP_30 and nP_50 solvents. All the lms cast from the nP_30 solvent show the highest intensity along the horizontal direction in the 2D SAXS data, which arises from domains that have a parallel orientation relative to the plane of the lm. Both of the three-layer (1000 µm3 and 100 µm3) lms, which have an ordered lamellar morphology in the bulk, show a much sharper contrast in intensity between the horizontal and vertical directions compared to the one-layer (1000 µm) lm, which has a poorly ordered bulk structure. This indicates that the three-layer lms have a larger population of highly oriented domains than the one-layer lms. On the other hand, the 2D SAXS data for lms cast from the neutral nP_50 solvent show the highest intensity along the vertical direction, arising from domains with a perpendicular orientation relative to the plane of the lm. These oriented layers could be present at either or both the polymer/air and polymer/Mylar interface. As only one preferred orientation is seen in each case, either a similar eect happens at both interfaces (controlled by solvent composition) or there is little surface-induced ordering at the Mylar interface. The preferred orientations observed for each solvent composition can be explained at the polymer/air interface based on the sharp change in solvent concentration at the bulk/skin interface: The selective nP_30 solvent would cause selective wetting of the non-polar tBS/HI domain at the skin/bulk interface, driving a preferred orientation of domains parallel to the plane of the lm in the skin layer, while the neutral nP_50 solvent could favor a perpendicular domain orientation. In a previous work, it was suggested that the formation of perpendicular orientation is favorable during solvent evaporation because

it avoids energetic penalties associated with chain stretching or compression and island/hole formation as the lm thickness continuously reduces.[55]

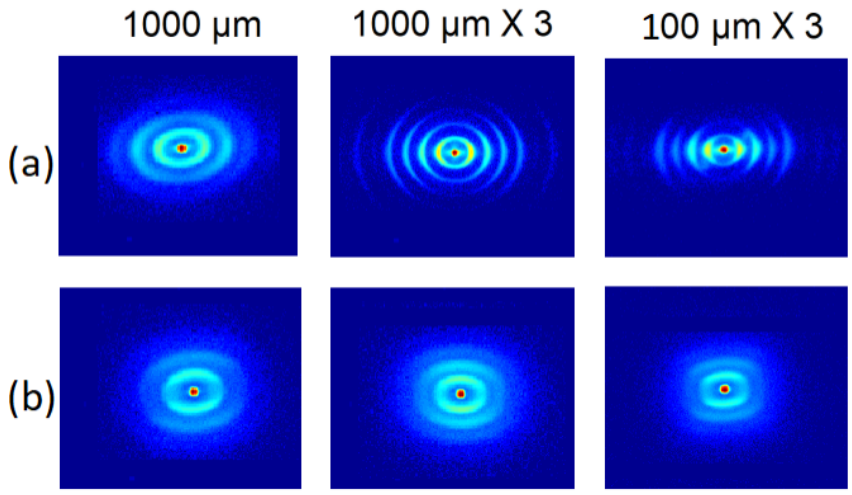


Figure 5: 2D SAXS data for measurements in the '||' conguration. Films cast from (a) nP_30 and (b) nP_50 solvents.

The elliptical pattern of the 2D SAXS proles indicates the domains oriented parallel to the plane of the lm show a reduced periodicity compared to domains oriented in other directions. Such reduction in periodicity in the vertical direction (along the thickness of the lm) has been observed in previous works with solvent cast lms[56] and after direct immersion annealing (DIA), which is a technique where the lm is immersed in a poor solvent that plasticizes the polymer to provide mobility for self assembly without dissolving the polymer.[57] For example, in block copolymer lms formed after rapid solvent removal following DIA, the periodicity of domains oriented parallel to the plane of the lm was reduced compared to thermally annealed lms.[57] During DIA there is reduction in the junction point density along the domain interface, and during rapid solvent removal the chains collapse in the vertical direction without signicantly altering the lateral chain density resulting in the reduced periodicity.[57] The same explanation could apply to solvent casting as well.

Figure 6 shows the 2D SAXS proles from measurements in the 'k' and '?' congurations for 1000 µm3 lms, cast using both nP_30 and nP_50 solvents. To illustrate the distinct domain orientations captured by the 'k' and '?' congurations more clearly, we also plot

the intensity of the rst-order ring as a function of azimuth angle. The data from the '?' conguration show a uniform intensity as a function of azimuth angle for lms cast using both nP_30 and nP_50 solvents, consistent with an un-oriented bulk structure. The data from the 'k' conguration show a clear variation in intensity along the azimuth, where the azimuth angles corresponding with maximum and minimum intensity are ipped for the lms cast from the nP_30 and nP_50 solvents. These trends reveal the presence of oriented domains in the lms, presumed to be located at the surface, and that the orientation direction is dependent on the solvent selectivity towards the blocks. When looking at the proles of scattered intensity as a function of azimuth angle, we note that scattering is about ten times higher for lms cast from nP_30 versus nP_50 solvent, despite the lms having similar thickness. This may be due to the fact that only a small fraction of the perpendicular domains in the nP_50 lms satisfy the Bragg condition (make a small angle with respect to the incident beam), or could reect a much thicker surface layer of parallel domains in the nP_30 lms.

Figure 6 also shows the 1D scattering data obtained by integrating intensity in the vertical and horizontal cut region of the rst-order ring from the 'k' conguration, as shown in Figure 2b. The 1D SAXS data obtained by azimuthal integration of the rst-order scattering ring from the '?' conguration is also shown in this gure. The 1D SAXS data from the '?' conguration and vertical cut of the 'k' conguration have identical proles and domain periodicities for lms cast from both nP_30 and nP_50 solvents, which makes sense because in the '?' conguration, the self-assembled domains that satisfy the Bragg condition are nearly perpendicular to the plane of the lm. For the lms cast from nP_30 solvent, the horizontal cut region of the 'k' conguration, which has higher intensity than the vertical region, shows a highly ordered lamellar morphology as evidenced by three well-dened higher order peaks. This indicates that the sequential deposition of layers using non-polar nP_30 solvent produces a self-assembled structure wherein a large fraction of domains are well-ordered lamellar sheets parallel to the plane of the lm, likely present in the skin layer. For

the nP_50 lms, the 1D scattering data from the horizontal cut region, which has lower intensity than the vertical region, shows a disordered structure characterized by a broad rst-order peak and oscillations in intensity at higher q values, indicating the presence of poorly ordered domains in the bulk of the lm.

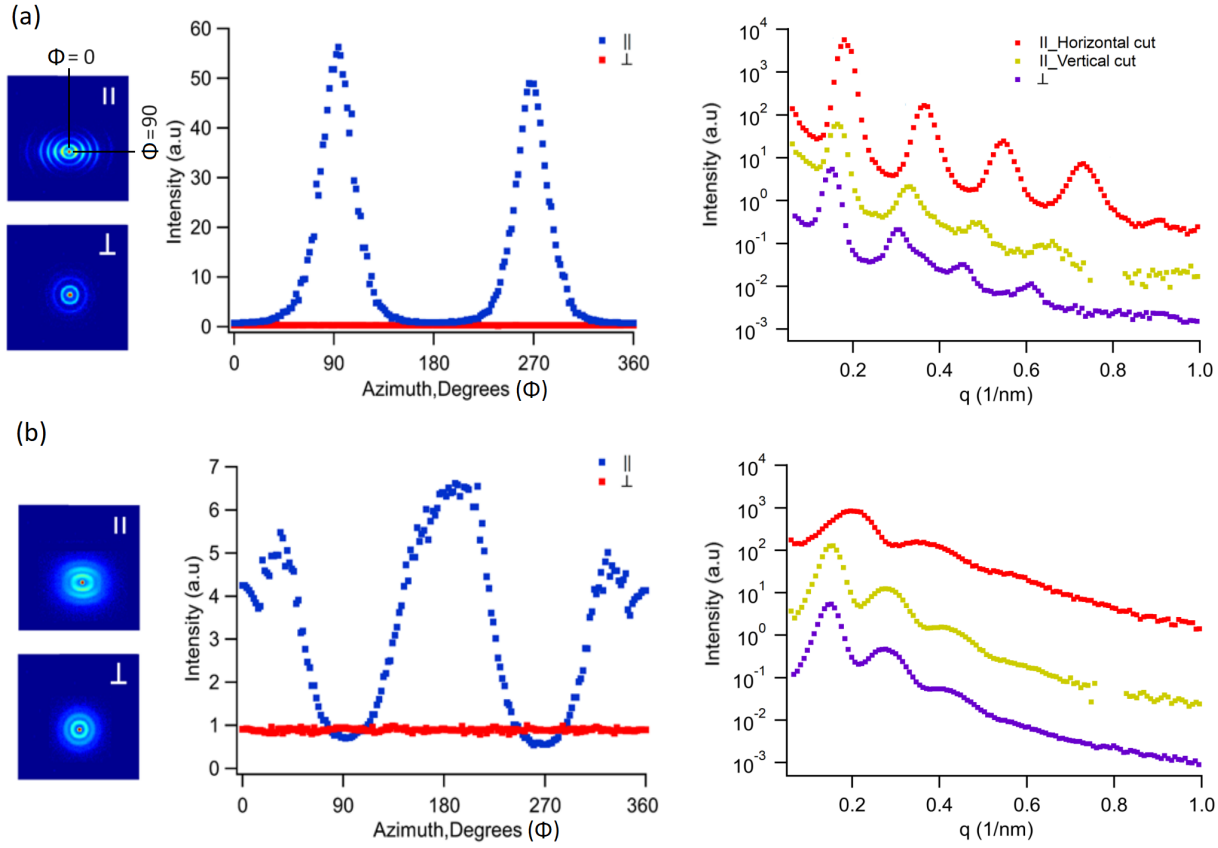


Figure 6: 2D scattering proles for the 1000 µm3 lms, corresponding plot of Intensity as a function of azimuth degrees, and 1 D scattering proles from azimuthal integration of intensity of the 2D scattering rings for ? conguration and intensity integration over horizontal and vertical cut region for the k conguration, lms cast with (a) nP_30 and (b) nP_50 solvents.

## Transport Measurements

The water and proton transport properties through the membrane are expected to be inu-enced by both bulk and surface morphologies. The morphology of the self-assembled struc-ture will impact the connectivity of the transport channels, which is an important parameter

for ion transport, and domain orientations in the surface region will impact transport properties that are controlled by surface resistance. When considering through-plane transport, a parallel domain orientation produces continuous layers of nonionic polymer that introduce resistance at the interface with an electrode. For in-plane transport, a parallel domain orientation may be preferable as it is less tortuous than perpendicular domains that form a network-like structure.

Figure 7 reports mass loss through the Nexar membranes from vials containing water, which results from the evaporation of water into the vapor head space followed by diusion through the permeable Nexar membranes. The mass loss shows an initial lag period followed by linear mass loss with time. The constant slope of mass loss with time, which is observed at longer times, is the steady state water vapor transport rate (WVTR) reported in Table 1. When WVTR is constant, the rates of water uptake and water loss through the membrane are equal. The initial lag time should be a function of the bulk morphology, domain orientations at the surface, as well as thicknesses of both the bulk and surface layers. The total lm thicknesses (bulk and surface) as well as the casting method are also reported in Table 1. While we do not have a direct measurement of the surface layer thickness, we expect that it increases with drying time and should therefore increase with the gap height used for casting.

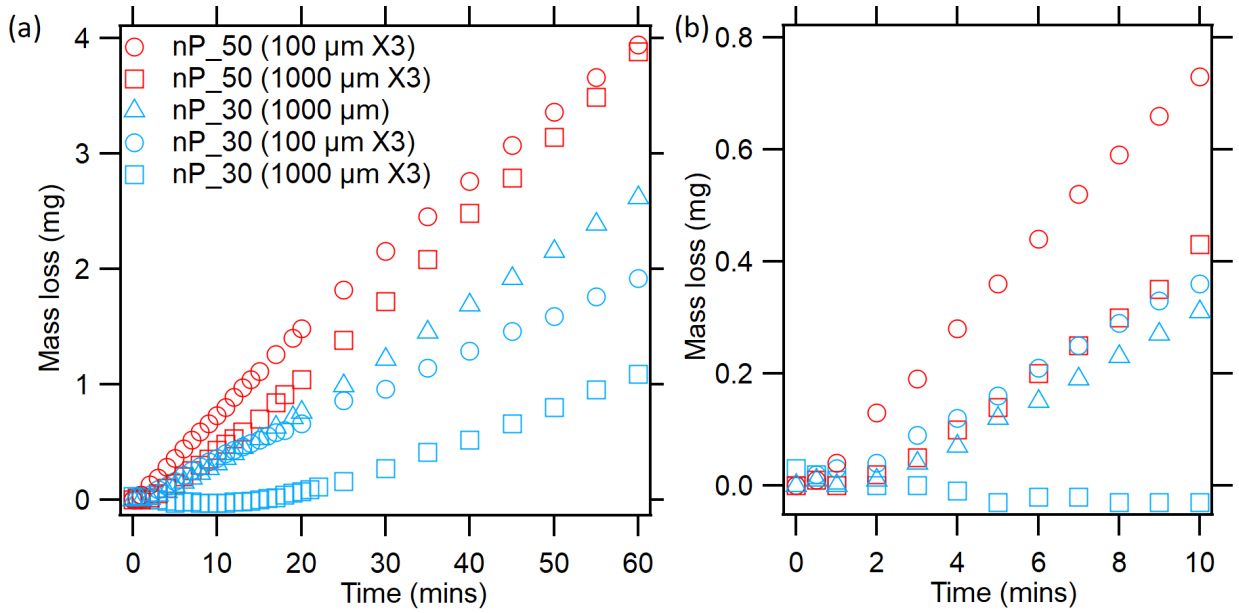


Figure 7: (a) Mass loss of water with time, for measurement of WVTR. (b) Enlarged region showing dierences in mass loss over the rst 10 minutes.

The lms cast from nP_30 solvent have ordered lamellae in bulk and parallel lamellae at the surface, and should therefore have the poorest water vapor transport properties due to longer grain boundaries in bulk and continuous non-ionic domains that act as barriers at the surface. The nP_30 (1000 µm3) lm shows the longest lag time, where mass loss begins after more than 10 min. The nP_30 (100 µm3) lm, which has similar bulk and surface structures as the nP_30 (1000 µm3) lm, has a lag time of about 2 min. The much longer lag time for the nP_30 (1000 µm3) lm compared to the nP_30 (100 µm3) lm can be explained by the dierence in lm thickness (300 µm versus 47 µm), as reported in Table 1. The drying time for a single layer of solution cast with a 1000 µm gap height is about 30 min, whereas the drying time for the same volume of solution cast using a 100 µm gap height is about 1 min. Thus the nP_30 (1000 µm3) lm, with a 300 µm dry thickness, has thicker bulk and surface layers compared to the nP_30 (100 µm3) lm, which has a nal dry thickness of 47 µm. The steady state WVTR, which is calculated from the constant slope of mass loss with time starting at 40 min, is reported in Table 1. Both the nP_30 (100 µm3) and nP_30 (1000 µm3) lms have similar WVTR slopes, as seen in Figure 7a,

Table 1: WVTR through dierent membranes.

| Sample | Film thickness (µm) | WVTR (mg/hr) |
|---|---|---|
| nP_50 (100 µm 3) | 34 | 3.5 |
| nP_50 (1000 µm 3) | 255 | 4.3 |
| nP_30 (1000 µm) | 111 | 2.8 |
| nP_30 (100 µm 3) | 47 | 1.9 |
| nP_30 (1000 µm 3) | 300 | 1.7 |

with values of 1.9 and 1.7 mg/hr respectively. This makes sense as the steady state WVTR should be a function of the lm structure and independent of thickness, and both these lms have similar bulk structure as shown in Figure 3 and similar surface structure and domain orientations as seen in Figures 6a and S5 b.

The lms cast from nP_50 solvent have disordered, network-like lamellar structure in bulk with a perpendicular domain orientation at the surface, and should therefore have the best water vapor transport properties due to high connectivity among ionic domains in bulk and low resistance to water uptake at the surface. The nP_50 (1000 µm3) lm shows a lag time of about 2 min, similar to that of the nP_30 (100 µm3) lm, despite the much higher lm thickness of 255 µm compared to the 47 µm thickness of nP_30 (100 µm3). The nP_50 (100 µm3) lm, which has a thickness of 34 µm, has a lag time of less than 1 min. The nP_50 (100 µm3) and nP_50 (1000 µm3) lms have similar WVTR slopes, as seen in Fig.7 a, with values of 3.5 and 4.3 mg/hr, respectively. This outcome is expected, as these lms have similar bulk structure and domain orientations as shown in Figures 3 and 5, respectively.

The nP_30 (1000 µm) lm has a thickness of 111 µm and shows a lag time of about 2 mins and WVTR of 2.8 mg/hr. This lm also shows domains oriented parallel to the plane of the lm, same as the three-layer nP_30 lms, but the three-layer lms showed a more pronounced orientation of domains than the one-layer lm as can be seen in Figure 5. Thus the nP_30 (1000 µm) lm, despite having more than twice the thickness of the nP_30 (100 µm3) lm, has a similar lag time. The intensity as a function of azimuth angle for the nP_30 (1000 µm) and nP_30 (100 µm3) lms plotted in Figure s7 clearly shows the

increase in the fraction of domains oriented parallel to the plane of the lm with sequential deposition of layers when cast using the nP_30 solvent. Figure S7 also reports the 1D SAXS proles integrated along the horizontal cut direction, which shows that the domains oriented parallel to the plane of the nP_30 (100 µm3) lms are well ordered lamellae. The three-layer nP_30 lms thus also have a lower equilibrium WVTR than the one-layer nP_30 (1000 µm) lm.

Next, we measured water uptake and proton conductivity in the through-lm direction at 35% RH. The orientation of domains on the surface of the lm would impact the water uptake by the lms, which is a critical parameter for the dissociation of the sulfonic acid group and thus proton transport through the lm. The water uptake corresponds to the wt% of water in the lms left at 35% RH for over an hour. The nP_30 (1000 µm3) lm showed a low water uptake of 25 wt% as compared to the nP_30 (1000 µm) and nP_50 (1000 µm3) lms that each had a water uptake of 50 wt%. As water uptake proceeds through the lm surface, the low water uptake by the nP_30 (1000 µm3) lms is limited by the highly ordered lamellar domains oriented parallel to the plane of the lm.

Proton conductivity in the through-lm direction for the nP_50 (1000 µm3) lm is three times higher than that of the nP_30 (1000 µm3) and the nP_30 (1000 µm) lms, even though these lms have the same water content. While this might be attributed to a surface eect, as the nP_30 lm with parallel lamellae at the surface could introduce resistance at the interface with electrode, a recent study has shown that through-lm measurements of the bulk ionic conductivity in block copolymer electrolytes are not sensitive to thin insulating interfacial layers.[58] However, from the TEM images of the bulk structures in Figure 4, we saw that nP_30 (1000 µm3) lms have a highly ordered lamellar structure while nP_50 (1000 µm3) lms have a poorly ordered network-like structure. The latter oers more interconnected pathways for transport, which can explain the higher proton conductivity.[16,20]

Table 2: Water content and proton conductivity through dierent polymer lm samples with dierent bulk and surface structures.

| Sample | Water wt% | Conductivity (mS/cm) | Bulk structure | Surface orientation |
|---|---|---|---|---|
| [1]nP_50 (1000 µm 3) | 50 | 0.45 | Network like | Perpendicular |
| [1]nP_30 (1000 µm 3) | 25 | 0.14 | Lamellar | Parallel |
| [1]nP_30 (1000 µm) | 50 | 0.14 | Poorly ordered | Parallel |
| [2]nP_50 (1000 µm 3) | 220 | 15.14 | Network like | Perpendicular |
| [2]nP_30 (1000 µm 3) | 133 | 6.99 | Lamellar | Parallel |
| [2]nP_30 (1000 µm) | 166 | 5.76 | Poorly ordered | Parallel |

[1]Equilibrated at 35% RH and 25C for 1 hr. [2] Soaked in DI water at 25C for 10 min

The nP_30 (1000 µm) lm which has a poorly ordered structure has a much higher water uptake compared to the nP_30 (1000 µm3) lms, which have a well-ordered lamellar structure. But both lms show similar through lm conductivity. Thus with similar water content, the poorly ordered structures with discontinuous SS domains would result in poor ionic conductivity compared to the highly ordered lamellar bulk structure. Table 2 also reports the through-lm proton conductivity of the lms after soaking in DI water. The lms after soaking in water had a much higher water content, increasing the proton conductivity by 35-50x. However, the high water content does not change the trends in proton conductivity as a function of lm structure.

## Conclusions

We examined the eects of solution-casting protocol on the bulk morphology and surface structure of an SPC, poly(tBS-HI-SS-HI-tBS). The lms were prepared using sequential bar-coating steps with varying bar gap heights, and solvent selectivity toward each block was controlled by solvent composition. The SPC concentration in solvent was xed at 15%. SAXS measurements showed that one-layer lms, prepared by bar coating a single layer of polymer solution using a gap heights of 1000 µm and 250 µm, produced a poorly-ordered lm structure irrespective of solvent selectivity. However, sequential deposition of two or more layers produced a 'templating' eect where the nal lm structure was correlated with

the solution-state structure.

When multilayer lms were cast from a solvent that is selective to the hydrophobic blocks, where the solution composition is near the boundary of lamellar and cylindrical phases, a lamellar morphology was formed where the extent of order in the bulk and at the surface improved with the number of layers. This nding demonstrates that when lms stay wet for a longer time, the SPC can better assemble into the preferred structure. We also found that lamellar domains adopt a parallel orientation at the surface of three-layer lms, an eect that is controlled by preferential interactions between the solvent and hydrophobic tBS/HI blocks, and is likely seeded at the boundary between the wet lm and drying skin layer. On the other hand, when multilayer lms were cast from a neutral solvent, which has no self-assembled structure in solution, the nal lms had a poorly ordered morphology irrespective of gap height or number of layers. This poorly ordered morphology was visualized through TEM measurements in a three-layer lm, which revealed a network-like structure of lamellar domains. Furthermore, the lamellar domains adopted a perpendicular orientation at the lm surface, an eect that minimizes entropic frustration during solvent evaporation.

The distinct bulk and surface morphologies have a strong inuence on transport properties. Through-plane measurements of bulk proton conductivity, which are insensitive to restructuring near a surface, demonstrate that the network-like morphology enhances the rate of proton transport relative to ordered lamellar grains. WVTR measurements, which are sensitive to both surface and bulk morphologies, are signicantly higher in lms with a network-like bulk structure and perpendicular domains at the surface. The lag time in WVTR measurements is directly correlated with the surface structure, as parallel lamellar orientations create resistance to water uptake, while the steady-state WVTR reects the available transport pathways in the bulk. Notably, the methodology described herein for 'templating' the solution-state structure in lms and tailoring domain orientations at surfaces can be used to optimize transport properties in other ionic block copolymer platforms.

## Acknowledgement

K.M. and G.E.S. thank the National Science Foundation for nancial support under Award No. DMR-1905487. SAXS measurements were enabled by the Major Research Instrumentation program of the National Science Foundation under Award No. DMR-1827474.

Supplementary Material. Solution phase diagram, SAXS data for all solutions, SAXS data for one-layer lm with 250 µm gap height and TEM data for select lms, SAXS data for drop cast lms dried by fast and slow solvent evaporation rate, GISAXS data for three-layer nP_30 amd nP_50 lms, 2D scattering proles for lms cast using nP_30 solvent along with intensity as a function of azimuth degrees, and 1D scattering proles. Nyquist plots for lms at 35% RH; and after soaking in DI water. Available free of charge at http:

# References


(1) Lehmann, M. L.; Yang, G.; Nanda, J.; Saito, T. Unraveling Ion Transport in Triuoromethanesulfonimide Pentablock Copolymer Membranes in Nonaqueous Electrolytes. Macromolecules 2022, 55, 77407751, DOI: 10.1021/acs.macromol.2c00513.

(2) Adhikari, S.; Pagels, M. K.; Jeon, J. Y.; Bae, C. Ionomers for electrochemical energy conversion & storage technologies. Polymer 2020, 211, 134, DOI: 10.1016/j.polymer.2020.123080.

(3) Meier-Haack, J.; Taeger, A.; Vogel, C.; Schlenstedt, K.; Lenk, W.; Lehmann, D. Membranes from sulfonated block copolymers for use in fuel cells. Separation and Purication Technology 2005, 41, 207220, DOI: 10.1016/j.seppur.2004.07.018.

(4) Bae, B.; Hoshi, T.; Miyatake, K.; Watanabe, M. Sulfonated block poly(arylene ether sulfone) membranes for fuel cell applications via oligomeric sulfonation. Macromolecules 2011, 44, 38843892, DOI: 10.1021/ma2000306.

(5) Hickner, M. A. Ion-containing polymers: new energy & clean water. Materials Today 2010, 13, 3441, DOI: 10.1016/S1369-7021(10)70082-1.

(6) Thomas, E. R.; Jain, A.; Mann, S. C.; Yang, Y.; Green, M. D.; Walker, S.; Perreault, F.; Lind, M. L.; Verduzco, R. Freestanding self-assembled sulfonated pentablock terpolymer membranes for high ux pervaporation desalination. Journal of Membrane Science 2020, 118460, DOI: 10.1016/j.memsci.2020.118460.

(7) Wang, Q.; Lu, Y.; Li, N. Preparation, characterization and performance of sulfonated poly(styrene-ethylene/butylene-styrene) block copolymer membranes for water desalination by pervaporation. Desalination 2016, 390, 3346, DOI: 10.1016/j.desal.2016.04.005.

(8) Geise, G. M.; Freeman, B. D.; Paul, D. R. Characterization of a sulfonated pentablock copolymer for desalination applications. Polymer 2010, 51, 58155822, DOI: 10.1016/j.polymer.2010.09.072.

(9) Fan, Y.; Zhang, M.; Moore, R. B.; Cornelius, C. J. Structure, physical properties, and molecule transport of gas, liquid, and ions within a pentablock copolymer. Journal of Membrane Science 2014, 464, 179187, DOI: 10.1016/j.memsci.2014.04.011.

(10) Filice, S.; D'Angelo, D.; Scarangella, A.; Iannazzo, D.; Compagnini, G.; Scalese, S. Highly eective and reusable sulfonated pentablock copolymer nanocomposites for water purication applications. RSC Advances 2017, 7, 4552145534, DOI: 10.1039/c7ra08000j.

(11) Buonomenna, M. G.; Yave, W.; Golemme, G. Some approaches for high performance polymer based membranes for gas separation: Block copolymers, carbon molecular sieves and mixed matrix membranes. RSC Advances 2012, 2, 1074510773, DOI: 10.1039/c2ra20748f.

(12) Truong, P. V.; Black, R. L.; Coote, J. P.; Lee, B.; Ardebili, H.; Stein, G. E. Systematic Approaches To Tailor the Morphologies and Transport Properties of Solution-Cast Sulfonated Pentablock Copolymers. ACS Applied Polymer Materials 2019, 1, 817, DOI: 10.1021/acsapm.8b00002.

(13) Kim, J.; Kim, B.; Jung, B.; Kang, Y. S.; Ha, H. Y.; Oh, I. H.; Ihn, K. J. Eect of casting solvent on morphology and physical properties of partially sulfonated polystyrene-block-poly(ethylene-ran-butylene)-block-polystyrene copolymers. Macromolecular Rapid Communications 2002, 23, 753756, DOI: 10.1002/1521-3927(20020901)23:13<753::AID-MARC753>3.0.CO;2-G.

(14) Kambe, Y.; Arges, C. G.; Czaplewski, D. A.; Dolejsi, M.; Krishnan, S.; Stoykovich, M. P.; De Pablo, J. J.; Nealey, P. F. Role of Defects in Ion Trans-

port in Block Copolymer Electrolytes. Nano Letters 2019, 19, 46844691, DOI: 10.1021/acs.nanolett.9b01758.

(15) Irwin, M. T.; Hickey, R. J.; Xie, S.; So, S.; Bates, F. S.; Lodge, T. P. Structure-conductivity relationships in ordered and disordered salt-doped diblock copolymer/homopolymer blends. Macromolecules 2016, 49, 69286939, DOI: 10.1021/acs.macromol.6b01553.

(16) Chintapalli, M.; Chen, X. C.; Thelen, J. L.; Teran, A. A.; Wang, X.; Garetz, B. A.; Balsara, N. P. Eect of grain size on the ionic conductivity of a block copolymer electrolyte. Macromolecules 2014, 47, 54245431, DOI: 10.1021/ma501202c.

(17) Arges, C. G.; Kambe, Y.; Dolejsi, M.; Wu, G. P.; Segal-Pertz, T.; Ren, J.; Cao, C.; Craig, G. S.; Nealey, P. F. Interconnected ionic domains enhance conductivity in microphase separated block copolymer electrolytes. Journal of Materials Chemistry A 2017, 5, 56195629, DOI: 10.1039/c6ta10838e.

(18) Yan, L.; Rank, C.; Mecking, S.; Winey, K. I. Gyroid and Other Ordered Morphologies in Single-Ion Conducting Polymers and Their Impact on Ion Conductivity. Journal of the American Chemical Society 2020, 142, 857866, DOI: 10.1021/jacs.9b09701.

(19) Ichikawa, T.; Yoshio, M.; Hamasaki, A.; Kagimoto, J.; Ohno, H.; Kato, T. 3D interconnected ionic nano-channels formed in polymer lms: Self-organization and polymerization of thermotropic bicontinuous cubic liquid crystals. Journal of the American Chemical Society 2011, 133, 21632169, DOI: 10.1021/ja106707z.

(20) Diederichsen, K. M.; Brow, R. R.; Stoykovich, M. P. Percolating transport and the conductive scaling relationship in lamellar block copolymers under connement. ACS Nano 2015, 9, 24652476, DOI: 10.1021/acsnano.5b01321.

(21) Campbell, I. P.; Lau, G. J.; Feaver, J. L.; Stoykovich, M. P. Network connectivity and

long-range continuity of lamellar morphologies in block copolymer thin lms. Macromolecules 2012, 45, 15871594, DOI: 10.1021/ma2025336.

(22) Shen, K. H.; Brown, J. R.; Hall, L. M. Diusion in Lamellae, Cylinders, and Double Gyroid Block Copolymer Nanostructures. ACS Macro Letters 2018, 7, 10921098, DOI: 10.1021/acsmacrolett.8b00506.

(23) Choi, J. H.; Ye, Y.; Elabd, Y. A.; Winey, K. I. Network structure and strong microphase separation for high ion conductivity in polymerized ionic liquid block copolymers. Macromolecules 2013, 46, 52905300, DOI: 10.1021/ma400562a.

(24) Wang, D.; Fan, Y. F.; Zhang, M.; Moore, R. B.; Cornelius, C. J. Ionomer solution to lm solidication dependence upon solvent type and its impact upon morphology and ion transport. European Polymer Journal 2017, 97, 169177, DOI: 10.1016/j.eurpolymj.2017.10.011.

(25) Huang, H.; Zhang, F.; Hu, Z.; Du, B.; He, T.; Lee, F. K.; Wang, Y.; Tsui, O. K. C. Study on the origin of inverted phase in drying solution-cast block copolymer lms. Macromolecules 2003, 36, 40844092, DOI: 10.1021/ma0217581.

(26) Huang, H.; Hu, Z.; Chen, Y.; Zhang, F.; Gong, Y.; He, T.; Wu, C. Eects of casting solvents on the formation of inverted phase in block copolymer thin lms. Macromolecules 2004, 37, 65236530, DOI: 10.1021/ma0498621.

(27) Elabd, Y. A.; Hickner, M. A. Block copolymers for fuel cells. Macromolecules 2011, 44, 111, DOI: 10.1021/ma101247c.

(28) Hwang, M.; Nixon, K.; Sun, R.; Willis, C.; Elabd, Y. A. Sulfonated pentablock terpolymers as membranes and ionomers in hydrogen fuel cells. Journal of Membrane Science 2021, 633, 119330, DOI: 10.1016/j.memsci.2021.119330.

(29) Choi, J. H.; Kota, A.; Winey, K. I. Micellar morphology in sulfonated pentablock copolymer solutions. Industrial and Engineering Chemistry Research 2010, 49, 12093 12097, DOI: 10.1021/ie1002476.

(30) Grin, P. J.; Salmon, G. B.; Ford, J.; Winey, K. I. Predicting the solution morphology of a sulfonated pentablock copolymer in binary solvent mixtures. Journal of Polymer Science, Part B: Polymer Physics 2016, 54, 254262, DOI: 10.1002/polb.23914.

(31) Mineart, K. P.; Ryan, J. J.; Appavou, M. S.; Lee, B.; Gradzielski, M.; Spontak, R. J. Self-Assembly of a Midblock-Sulfonated Pentablock Copolymer in Mixed Organic Solvents: A Combined SAXS and SANS Analysis. Langmuir 2019, 35, 10321039, DOI: 10.1021/acs.langmuir.8b03825.

(32) Etampawala, T. N.; Aryal, D.; Osti, N. C.; He, L.; Heller, W. T.; Willis, C. L.; Grest, G. S.; Perahia, D. Association of a multifunctional ionic block copolymer in a selective solvent. Journal of Chemical Physics 2016, 145, DOI: 10.1063/1.4967291.

(33) Mineart, K. P.; Jiang, X.; Jinnai, H.; Takahara, A.; Spontak, R. J. Morphological investigation of midblock-sulfonated block ionomers prepared from solvents differing in polarity. Macromolecular Rapid Communications 2015, 36, 432438, DOI: 10.1002/marc.201400627.

(34) Zheng, W.; Cornelius, C. J. Solvent tunable multi-block ionomer morphology and its relationship to modulus, water swelling, directionally dependent ion transport, and actuator performance. Polymer 2016, 103, 104111, DOI: 10.1016/j.polymer.2016.09.055.

(35) Jain, A.; Weathers, C.; Kim, J.; Meyer, M. D.; Walker, W. S.; Li, Q.; Verduzco, R. Self assembled, sulfonated pentablock copolymer cation exchange coatings for membrane capacitive deionization. Molecular Systems Design and Engineering 2019, 4, 348356, DOI: 10.1039/c8me00115d.

(36) Madathil, K.; Lantz, K. A.; Stek, M.; Stein, G. E. Eects of Trace Water on Self-Assembly of Sulfonated Block Copolymers during Solution Processing. ACS Applied Polymer Materials 2020, 2, 48934901, DOI: 10.1021/acsapm.0c00806.

(37) Choi, J. H.; Willis, C. L.; Winey, K. I. Structure-property relationship in sulfonated pentablock copolymers. Journal of Membrane Science 2012, 394-395, 169174, DOI: 10.1016/j.memsci.2011.12.036.

(38) Cheng, S.; Smith, D. M.; Pan, Q.; Wang, S.; Li, C. Y. Anisotropic ion transport in nanostructured solid polymer electrolytes. RSC Advances 2015, 5, 4879348810, DOI: 10.1039/c5ra05240h.

(39) Park, M. J.; Balsara, N. P. Anisotropie proton conduction in aligned block copolymer electrolyte membranes at equilibrium with humid air. Macromolecules 2010, 43, 292 298, DOI: 10.1021/ma901980b.

(40) Majewski, P. W.; Gopinadhan, M.; Jang, W. S.; Lutkenhaus, J. L.; Osuji, C. O. Anisotropic ionic conductivity in block copolymer membranes by magnetic eld alignment. Journal of the American Chemical Society 2010, 132, 1751617522, DOI: 10.1021/ja107309p.

(41) Majewski, P. W.; Gopinadhan, M.; Osuji, C. O. The eects of magnetic eld alignment on lithium ion transport in a polymer electrolyte membrane with lamellar morphology. Polymers 2019, 11, DOI: 10.3390/polym11050887.

(42) Gwee, L.; Choi, J. H.; Winey, K. I.; Elabd, Y. A. Block copolymer/ionic liquid lms: The eect of ionic liquid composition on morphology and ion conduction. Polymer 2010, 51, 55165524, DOI: 10.1016/j.polymer.2010.09.026.

(43) Young, W. S.; Epps, T. H. Ionic conductivities of block copolymer electrolytes with various conducting pathways: Sample preparation and processing considerations. Macromolecules 2012, 45, 46894697, DOI: 10.1021/ma300362f.

(44) Robertson, M.; Zhou, Q.; Ye, C.; Qiang, Z. Developing Anisotropy in Self-Assembled Block Copolymers: Methods, Properties, and Applications. Macromolecular Rapid Communications 2021, 42, 132, DOI: 10.1002/marc.202100300.

(45) Kim, S. Y.; Yoon, E.; Joo, T.; Park, M. J. Morphology and conductivity in ionic liquid incorporated sulfonated block copolymers. Macromolecules 2011, 44, 52895298, DOI: 10.1021/ma200278c.

(46) Kim, S. Y.; Kim, S.; Park, M. J. Enhanced proton transport in nanostructured polymer electrolyte/ionic liquid membranes under water-free conditions. Nature Communications 2010, 1, DOI: 10.1038/ncomms1086.

(47) Zheng, W.; Liu, C. H.; Nieh, M. P.; Cornelius, C. J. Sulfonated Pentablock Copolymer Membrane Morphological Anisotropy and Its Impact on Dimensional Swelling, Proton Conductivity, and the Transport of Protons and Water. Macromolecules 2022, 55, 92699281, DOI: 10.1021/acs.macromol.2c00987.

(48) Willis, C. L.; Handlin, D. L.; Trenor, S. R.; Mather, B. D. Sulfonated block copolymers, method for making same, and various uses for such block copolymers. United States Patent Application 2007, US 2007/0021569 A1.

(49) Truong, P. V.; Shingleton, S.; Kammoun, M.; Black, R. L.; Charendo, M.; Willis, C.; Ardebili, H.; Stein, G. E. Structure and Properties of Sulfonated Pentablock Terpolymer Films as a Function of Wet-Dry Cycles. Macromolecules 2018, 51, 22032215, DOI: 10.1021/acs.macromol.8b00194.

(50) Grin, P. J.; Salmon, G. B.; Ford, J.; Winey, K. I. Predicting the solution morphology of a sulfonated pentablock copolymer in binary solvent mixtures. Journal of Polymer Science, Part B: Polymer Physics 2016, 54, 254262, DOI: 10.1002/polb.23914.

(51) Heinzer, M. J.; Han, S.; Pople, J. A.; Baird, D. G.; Martin, S. M. In Situ Measurement of Block Copolymer Ordering Kinetics during the Drying of Solution-Cast

Films Using Small-Angle X-ray Scattering. Macromolecules 2012, 45, 34713479, DOI: 10.1021/ma2026435.

(52) Ghoshal, S.; Denner, P.; Stapf, S.; Mattea, C. Study of the Formation of Poly ( vinyl alcohol ) Films. Macromolecules 2012, 45, 19131923, DOI: 10.1021/ma2023292.

(53) G.Kim,; M.Libera, Morphological development in solvent-cast polystyrene-polybutadiene-polystyrene (SBS). Macromolecules 1998, 31, 25692577.

(54) Berezkin, A. V.; Papadakis, C. M.; Potemkin, I. I. Vertical domain orientation in cylinder-forming diblock copolymer lms upon solvent vapor annealing. Macromolecules 2016, 49, 415424.

(55) Albert, J. N. L.; Young, W.-S.; Lewis III, R. L.; Bogart, T. D.; Smith, J. R.; Epps III, T. H. Systematic study on the eect of solvent removal rate on the morphology of solvent vapor annealed ABA triblock copolymer thin lms. ACS Nano 2012, 6, 45966.

(56) Heinzer, M. J.; Han, S.; Pople, J. A.; Baird, D. G.; Martin, S. M. In situ tracking of microstructure spacing and ordered domain compression during the drying of solution-cast block copolymer lms using small-angle X-ray scattering. Macromolecules 2012, 45, 34803486, DOI: 10.1021/ma2026435.

(57) Longanecker, M.; Modi, A.; Dobrynin, A.; Kim, S.; Yuan, G.; Jones, R.; Satija, S.; Bang, J.; Karim, A. Reduced domain size and interfacial width in fast ordering nanolled block copolymer lms by direct immersion annealing. Macromolecules 2016, 49, 85638571, DOI: 10.1021/acs.macromol.6b01690.

(58) Coote, J. P.; Adotey, S. K. J.; Sangoro, J. R.; Stein, G. E. Interfacial Eects in Conductivity Measurements of Block Copolymer Electrolytes. ACS Polym. Au 2023, 3, 331343, DOI: 10.1021/acspolymersau.2c00068.